Chapter 5 – Laser Ablation at the Solid/Liquid Interface

In this chapter the results of laser ablation of various materials under various liquids will be reported. In the first section the manufacture of diamond by the laser ablation of graphite under water and under cyclohexane will be discussed. From the results of this work the ablation of both white and red phosphorus under various carbon containing liquids will be presented. From this it will be seen that crystalline carbon phosphide may have been observed for the first time. Finally suggestions as to how the method could be improved will be put forward.

5.1 Graphite Ablated Under Oxygen and Carbon Containing Liquids

In this section the results of the ablation of graphite under water and under cyclohexane will be presented. Wang and Yang *et al*[1-3] carried out the ablation of graphite under water. They found that diamond was produced and concluded that this was due to the OH and O species present in the breakdown products of water that etched away non sp^3 carbon – carbon hybrids. The aim of this study was to reproduce these results and then try to produce diamond from a liquid that does not contain O. Cyclohexane was chosen, as it has a relatively high boiling point (~81 ºC), its relative safety (compared to liquids such as benzene and toluene) and of course it contains no O. It can be seen that if diamond can be produced under these conditions it is not possible for O and OH to play a role in the production of diamond. It would therefore be more likely that diamond is formed under HPHT conditions. Knowing this, it

would be possible to attempt to produce crystalline carbon phosphide in an HPHT environment using this technique. Unless otherwise stated these ablations were carried out with the 1st harmonic of the YAG laser (532 nm).

5.1.1 Ablation of Graphite Under Water

The suspension produced from the laser ablation of graphite under water was clear in appearance, containing a visible suspended black solid. After leaving the suspension to settle overnight the solid sank to the bottom of the sample vial, care was always taken when preparing TEM grids to agitate the suspension to ensure that some of these particles were analysed. If the suspensions were not shaken, the TEM revealed that some solid still remained suspended in the liquid. These pieces were usually very small (<500 nm).

Figure 5.1 shows a TEM micrograph of a sample produced by the ablation of graphite under water. It can be seen that the left half of the micrograph shows a thin section, with sheet like layers and wave like features. From Selected Area Electron Diffraction (SAED) patterns it has been determined that these are graphite sheets (Figure 5.4 and Figure 5.5). It can be seen from the grain boundaries that the graphite is nano/microcrystalline. On the right hand side of this micrograph there is an area that looks very different. If a SAED pattern is taken (shown in Figure 5.2) it is possible to determine whether it is diamond, or graphite (or indeed any other crystalline material). This can be qualitatively done using the known diffraction patterns as shown in Figure 5.6 and comparing the intensity and spacing of the peaks with the intensity of the SAED diffraction pattern. There is also a quantitative method of doing this; if the ring pattern on the SAED is measured as radius from the centre of

the pattern, this can be compared to the known *d*-spacings of diamond. From the *d*-spacings the lattice parameters *a, b and c* (for cubic *a=b=c*) can be determined. In this study the computer program 'Process Diffraction'[4], was used to measure the radial distribution of darkness from the centre spot. The program outputted *d*-spacings directly.

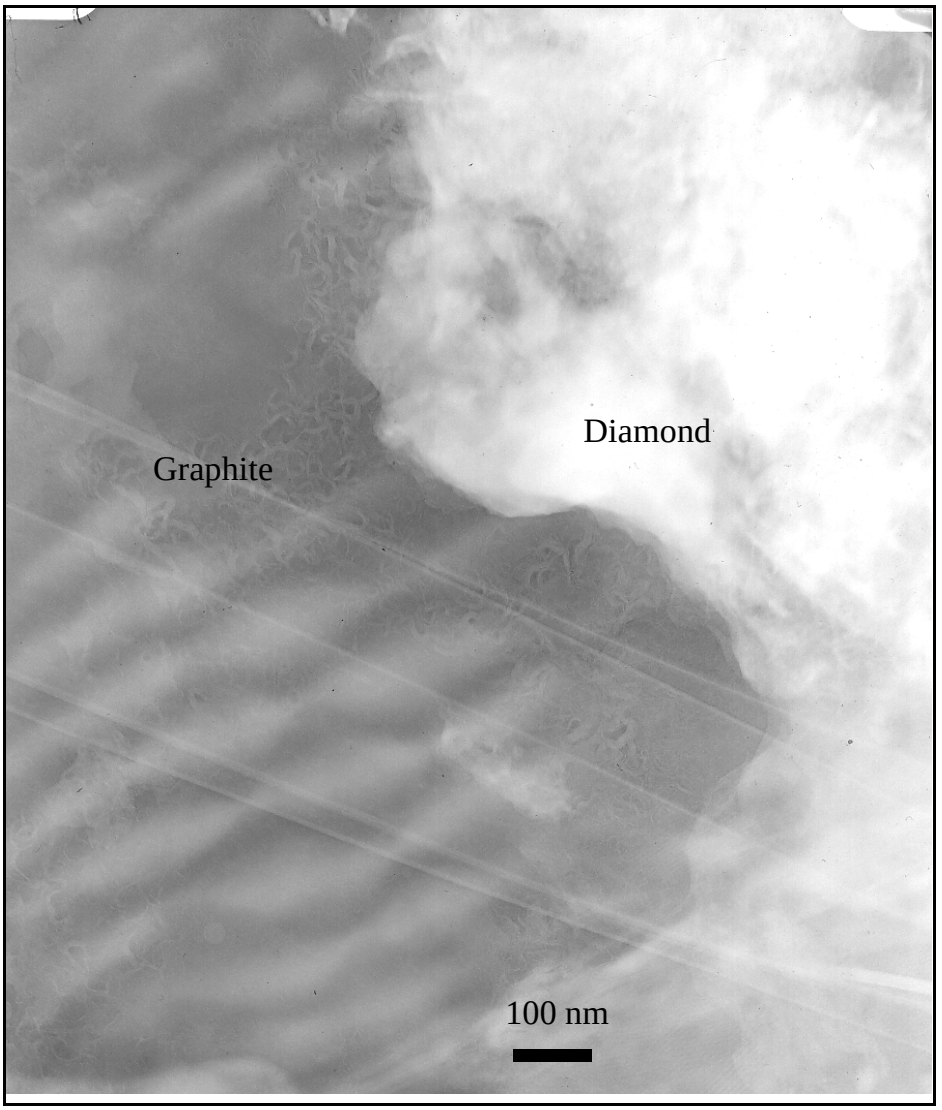

Figure 5.1: TEM micrograph of the an area containing diamond from a sample made by graphite being ablated under water.

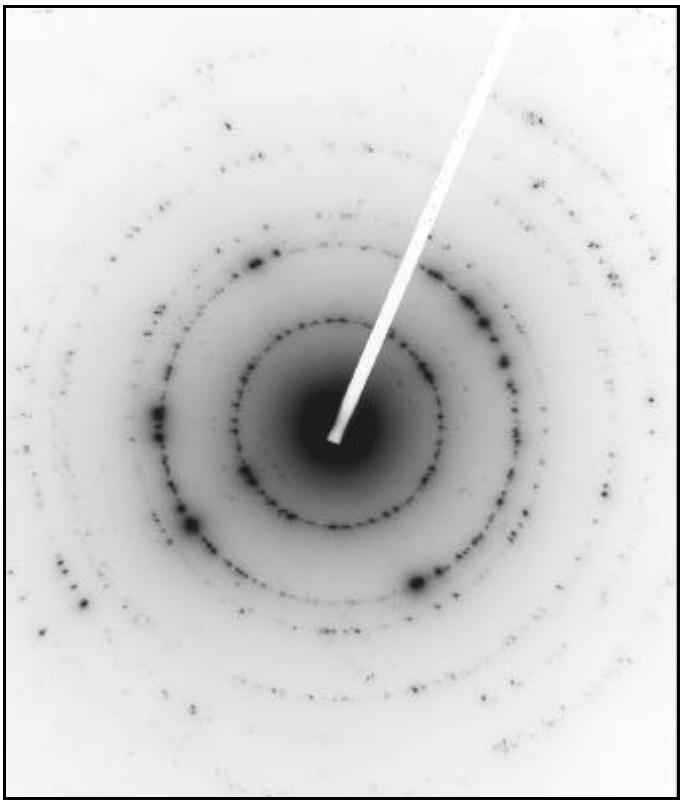

Figure 5.2: A Selected Area Electron Diffraction pattern of diamond crystals from the sample shown in Figure 5.1. This SAED was taken with a camera length of 1000 mm.

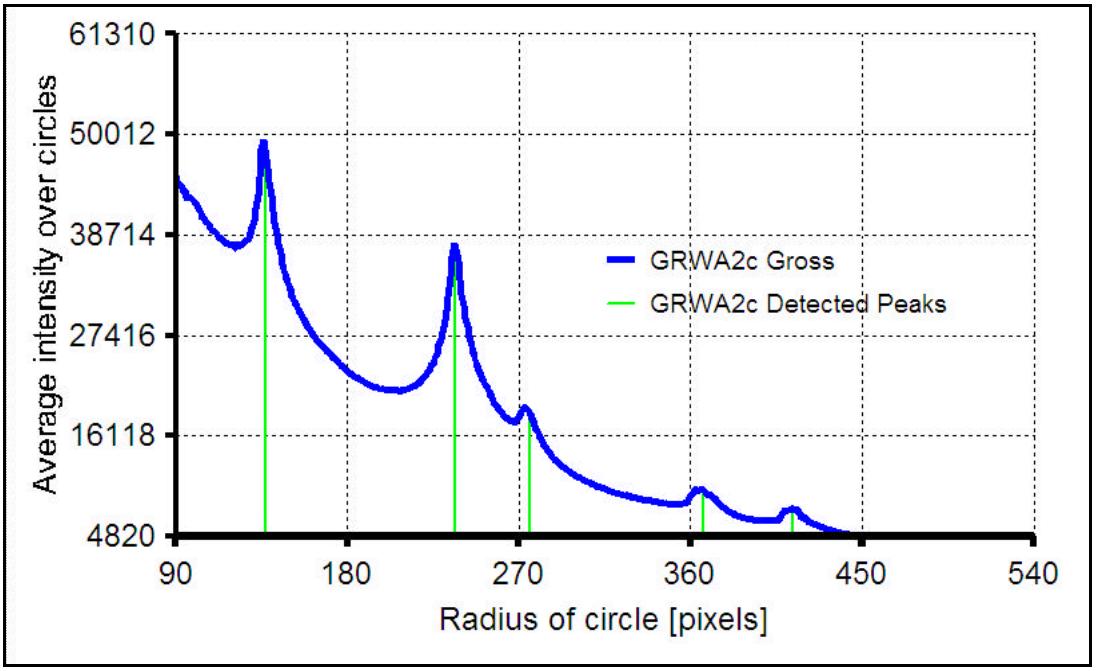

Figure 5.3: The intensity against the radius of the circle from the above SAED pattern, this was produced using ProcessDiffraction[4]

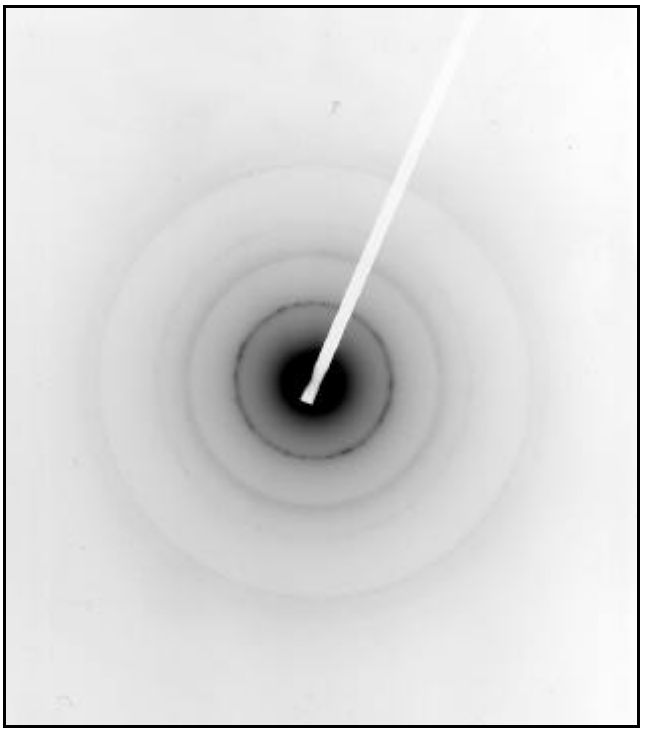

Figure 5.4: Diffraction pattern from the graphite area in Figure 5.1. This SAED was taken with a camera length of 1200 mm.

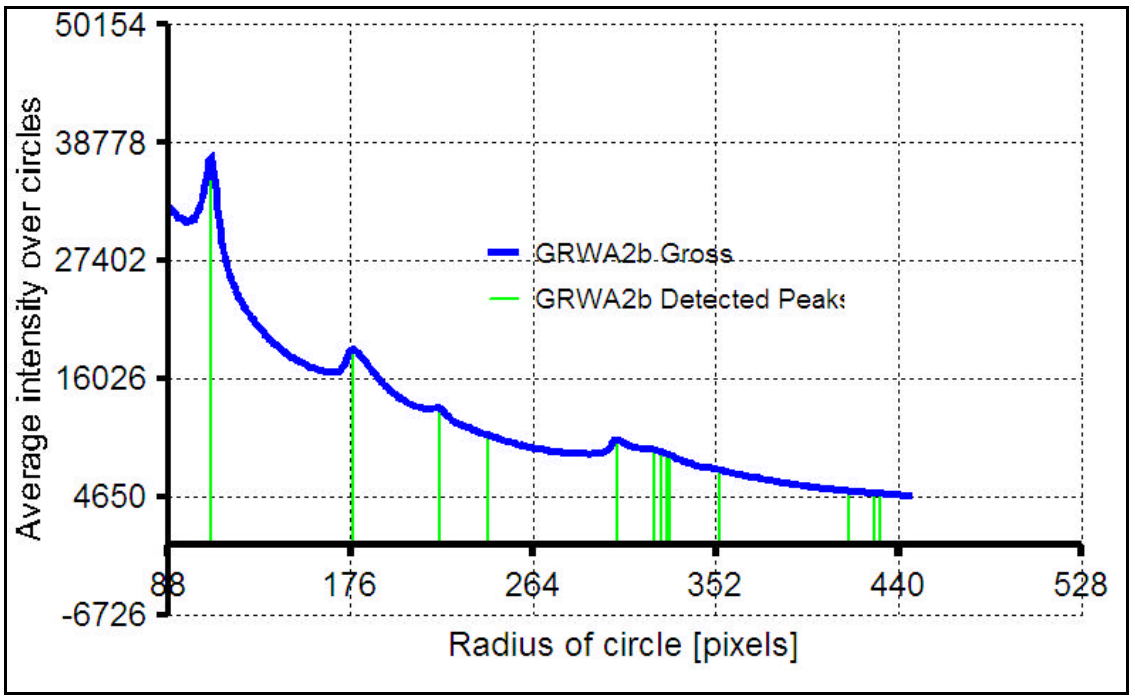

Figure 5.5: The intensity against the radius of the circle from the above SAED pattern. This was produced using Process Diffraction[4]

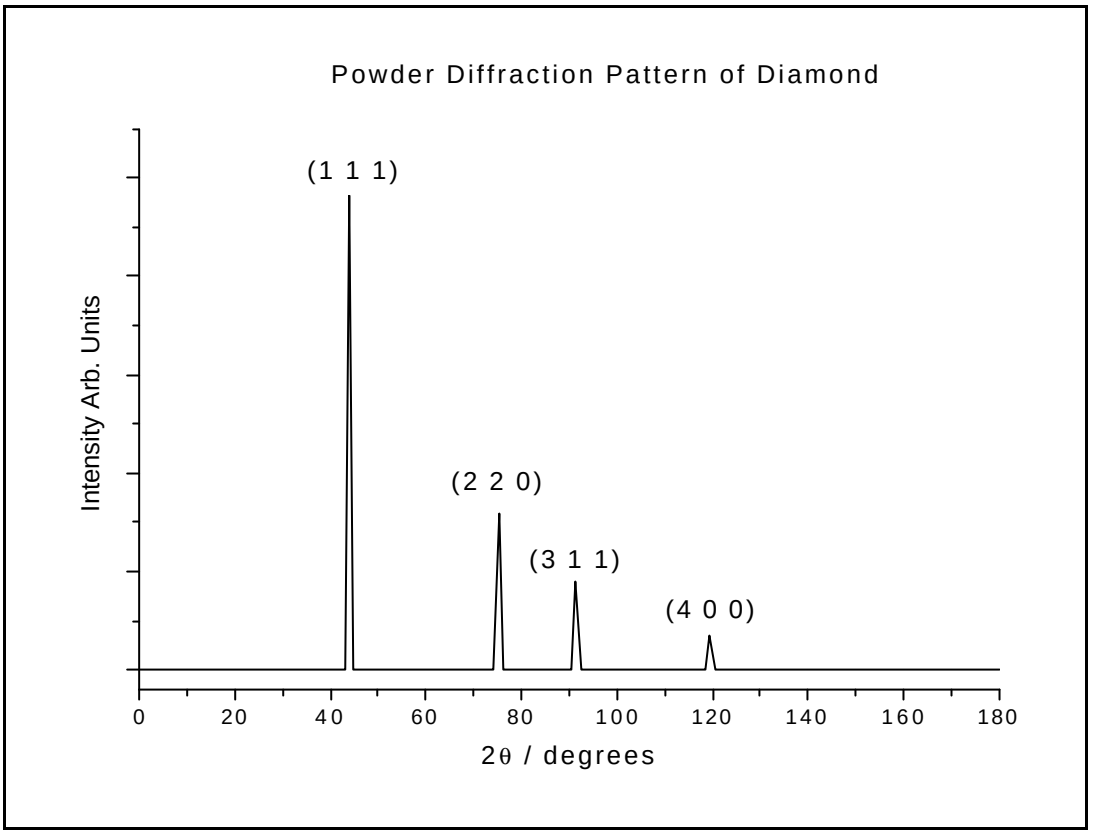

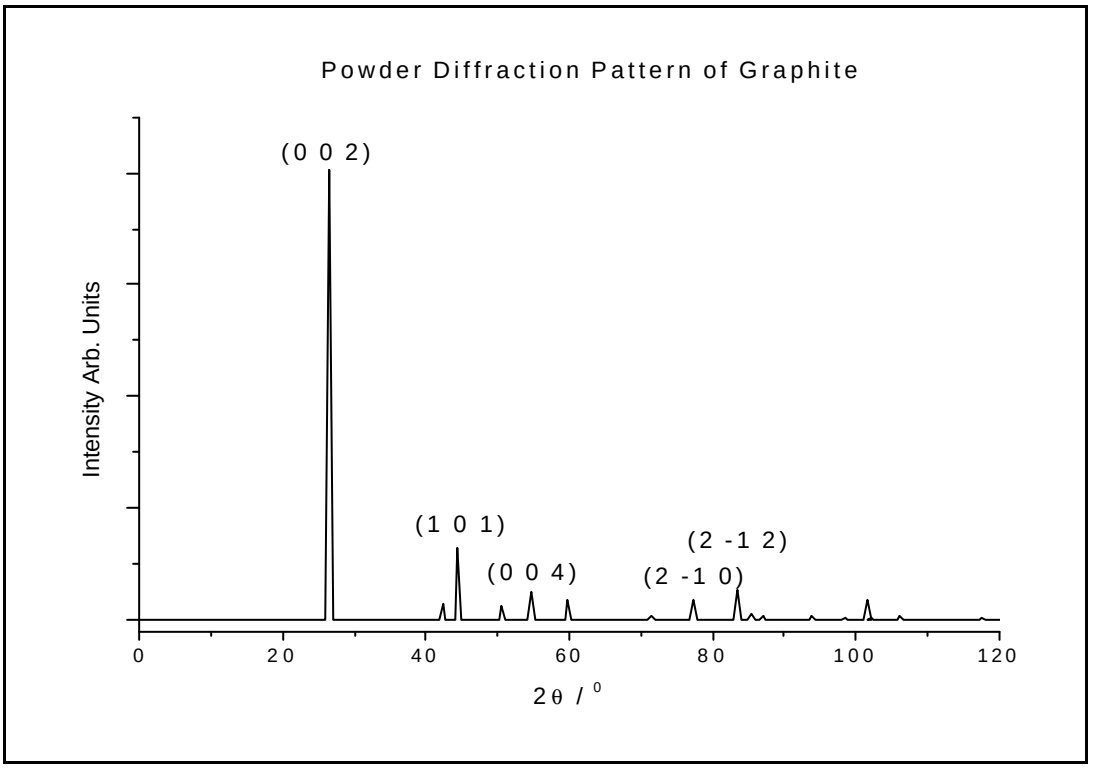

Figure 5.6: The expected diffraction patterns for diamond and graphite generated by CaRIne v3.1[5]

Figure 5.3 shows the radial distribution of intensity of the SAED pattern shown in Figure 5.2. It can be seen that the areas of high intensity have been fitted as peaks, the position of these peaks are related to the *d*-spacing by Equation 5.1, where *d* is the *d*-spacing, ? is the wavelength of the electron beam (calculated by Process Diffraction, which takes into account the relativistic effects of the high energy electrons on the wavelength), *l* is the camera length (in mm) and *r* is radius of the circles in the diffraction pattern (in mm). This calculation is automatically done in Process Diffraction.

$$d = \frac{l\,l}{r}$$

Equation 5.1

Table 5.1 shows the *d*-spacings calculated for the SAED pattern shown in Figure 5.2 and the *d*-spacings for diamond and graphite. It can be seen that the *d*-spacings list for diamond fits well, whereas that for graphite does not fit particularly well.

Experimental		Diamond		Graphite	
Plane	*d*-spacing	Plane	*d*-spacing	Plane	*d*-spacing
?	2.156	<1 1 1>	2.059	<0 0 2>	3.355
?	1.25	<2 2 0>	1.261	<1 0 0>	2.134
?	1.074	<3 1 1>	1.075	<1 0 1>	2.034
?	0.807	<3 3 1>	0.818	<1 0 2>	1.801

Table 5.1: The *d*-spacings for the experimental data (calculated by Process Diffraction), diamond and graphite (calculated using CaRine v3.1)

The lattice parameters *a*, *b* and *c*, can be calculated for each plane, to confirm that the plane assignment is correct. This is done using Equation 5.2 rearranged to Equation 5.3, where d_{hkl} is the *d*-spacing, *a* is the lattice parameter and *h*, *k* and *l* are the Miller indices of the plane that is being calculated.

$$d_{<hkl>} = \sqrt{\frac{a^2}{h^2 + k^2 + l^2}}$$

Equation 5.2

If Equation 5.2 is rearranged:

$$d_{<hkl>} = \frac{a}{\sqrt{h^2 + k^2 + l^2}}$$

$$a = d_{<hkl>} \sqrt{h^2 + k^2 + l^2}$$

Equation 5.3

This has been done for these data and the results are shown in Table 5.2. It shows that there is a good agreement between the experimentally calculated and the known lattice parameter for diamond (3.567 Å – Fayos *et al*[6]). It is therefore clear that diamond has been produced.

Plane	*d-spacing*	*a / Å*
<1 1 1>	2.156	3.73
<2 2 0>	1.25	3.54
<3 1 1>	1.074	3.56
<3 3 1>	0.807	3.52

Table 5.2: lattice parameter (*a*) calculated for the experimental data shown in Table 5.1.

The diamond that has been produced by this technique has a very small crystal size, this is apparent even when the magnification of the microscope exceeds 200 k X magnification. This is why the SAED is a ring pattern as opposed to a spot pattern. Also it is evident from analysing the sample that most of the sample (around 95%) remained unchanged as graphite. If a way of etching away non-diamond graphite were found, this may be a useful method for producing aqueous suspensions of

nanocrystalline diamond relatively simply and cheaply. Attempts were made to etch away graphite by refluxing the mixture in concentrated nitric acid for two hours, but no etching was observed.

5.1.2 Ablation of Graphite Under Cyclohexane

The suspensions produced in this study were yellow in colour and were transparent. There was suspended black solid present in each sample. If left overnight this sank to the bottom. Care was taken to ensure that before analysis all samples were agitated. If the samples were not agitated the TEM revealed that very small particles were still present in the liquid. It is thought that the yellow colour may have been due to either the presence of stable nanoparticles in solution or due to the breakdown products of the cyclohexane by the laser radiation. Toyota *et al*[7] have previously observed that among other products exposure of cyclohexane to a fundamental Nd:YAG pulse caused hydrogen, methane, ethane, acetylene and ethylene, as well as other non volatile products, to be produced. The laser used in this study was at the 1st harmonic, but the products are likely to be similar.

Figure 5.7 shows a TEM micrograph of a sample produced by ablation of graphite under cyclohexane. It can be seen that the micrograph is very different to that in Figure 5.1. This is thought to be due to the non-volatile products, which would form an amorphous film after the cyclohexane and more volatile components of the mixture were evaporated. Indeed when analysing any samples with cyclohexane as the liquid, care had to be taken as the electron beam heated the product and the lighter components boiled off.

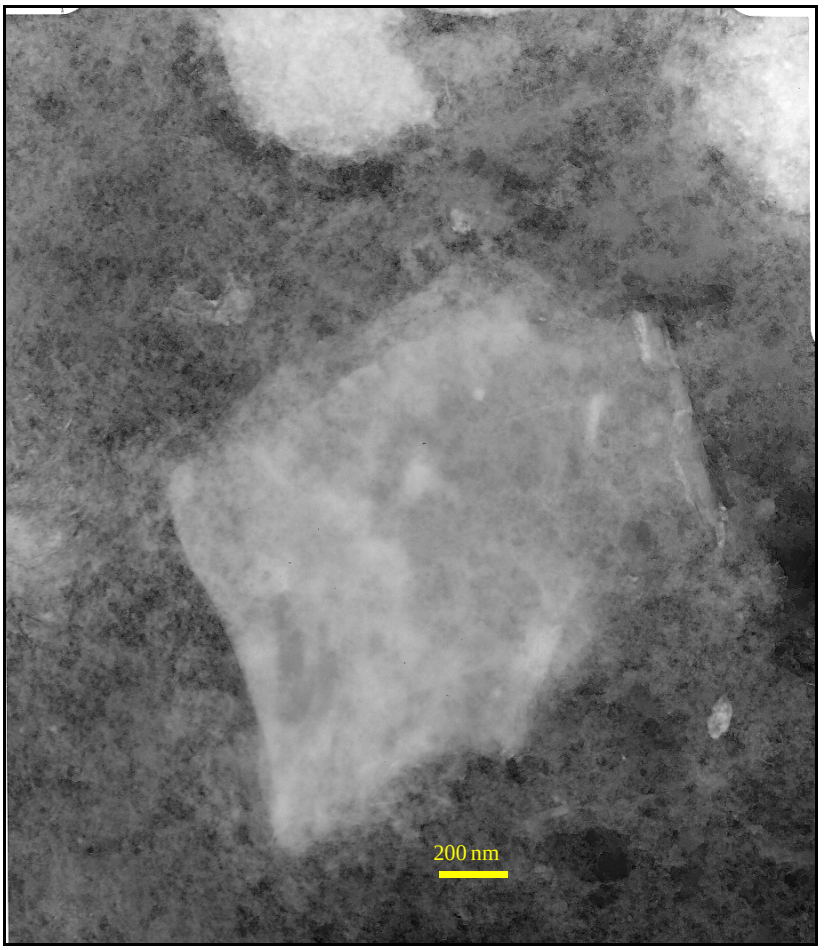

Figure 5.7: TEM micrograph of a sample produced by ablation of graphite under cyclohexane.

Figure 5.8 shows an SAED of a small area of the material shown in Figure 5.7. Figure 5.9 shows the radial distribution of the rings. It can be seen that even though it has the same ring pattern distribution as that shown in Figure 5.2 the pattern has solid rings as opposed to "dotted" rings. This is due to more randomly orientated crystals than in the other case. It may also indicate that the crystal size is smaller than those shown previously. As mentioned above an attempt was made to measure the crystals by trying to find the grain boundaries. This was found to be difficult, as even at high resolutions (>100 k magnification), individual crystals could not be picked out from the bulk.

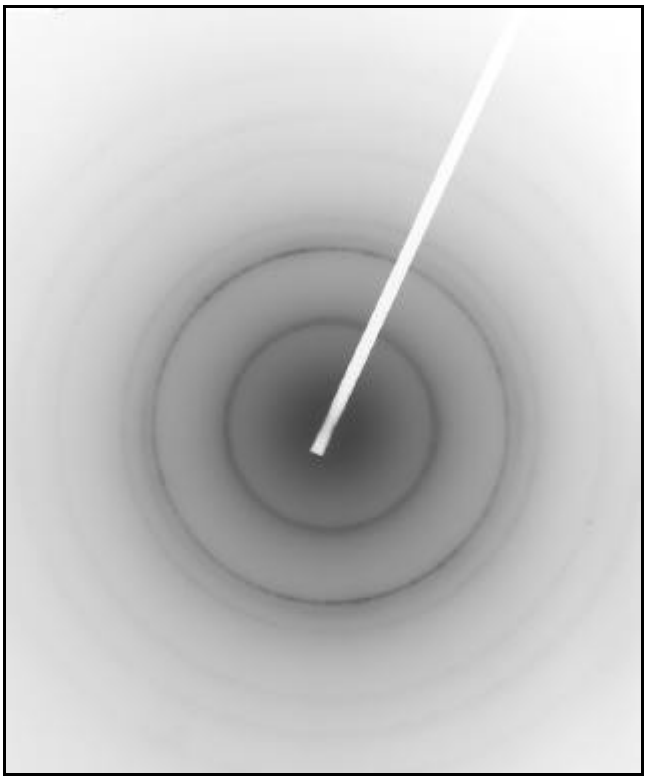

Figure 5.8: SAED of a small area of Figure 5.7. This sample was produced by ablation of graphite under cyclohexane. The camera length was 1000 mm.

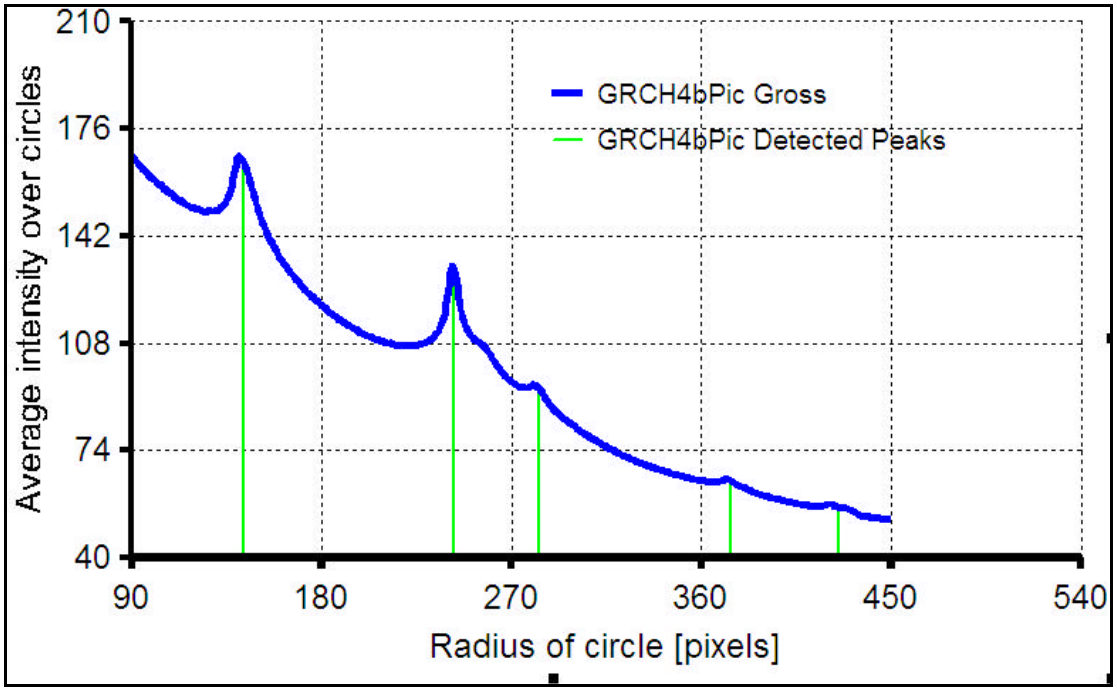

Figure 5.9: The intensity against the radius of the circle from the above SAED pattern, this was produced using the Process Diffraction computer program.

Table 5.3 shows the *d*-spacings of the material analysed in the SAED shown in Figure 5.8. It can be seen that the *d*-spacings correspond well to those of diamond. The table also shows the correlation of the experimental data with the lattice parameter. This also corresponded well to the known lattice parameter of diamond showing that the plane assignments and spacings are correct.

Experimental			Diamond	
Plane	*d*-spacing	*a* / Å	Plane	*d*-spacing
<1 1 1>	2.072	3.59	<1 1 1>	2.059
<2 2 0>	1.221	3.45	<2 2 0>	1.261
<3 1 1>	1.046	3.47	<3 1 1>	1.075
<3 3 1>	0.791	3.45	<3 3 1>	0.818

Table 5.3: *d*-spacings and lattice parameter calculated from the SAED shown in Figure 5.8.

Laser Raman analysis of the material was difficult to perform as the minimum spot size of the laser Raman spectrometer was approximately 1 µm and the crystal sizes were significantly smaller than this. A laser Raman spectrum is shown in Figure 5.10. It shows a spectrum typical of disordered graphite, but at around 1150 cm^{-1} there is a broad peak that several authors have previously assigned to trans-polyacetylene[8,9]. However, this peak is also commonly seen in nanocrystalline diamond films grown by gas phase CVD methods[8].

From the above results it has been shown that diamond has been formed from graphite being ablated under cyclohexane. This conflicts with the views put forward by Wang and Yang *et al*, that the formation of diamond from graphite being ablated under water is due to OH and O containing species etching away non-diamond carbon. It is much more likely from this that the mechanism is HPHT.

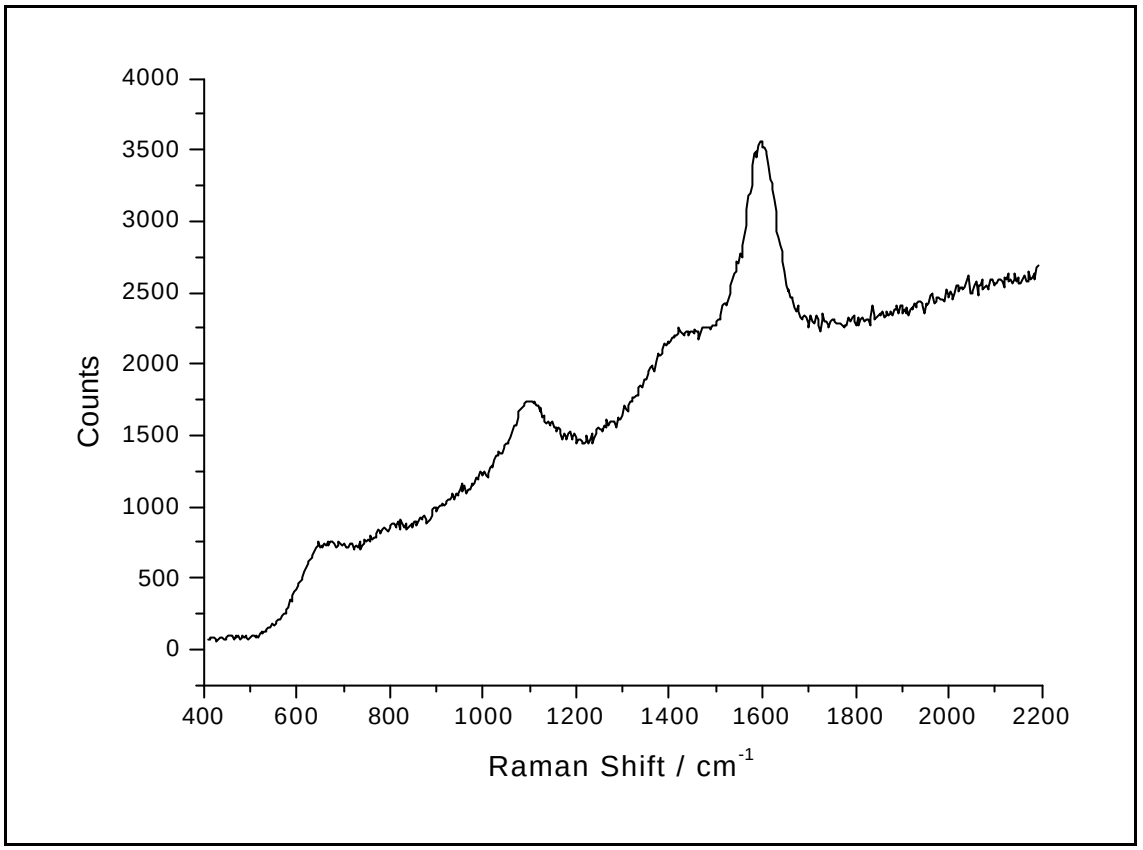

Figure 5.10: Laser Raman Spectrum taken with a 325 nm laser, of the dried suspension produced by ablation of graphite under cyclohexane.

5.1.3 Optical Emission Spectra of the Ablation Plume

Figure 5.11 shows OES spectra of the light emission from graphite being ablated under water and cyclohexane. It can be seen that there are several prominent peaks, mostly from H. This is direct evidence for the breakdown of the solvent. The broad peak at around 650 nm has been assigned to the Balmer-a hydrogen emission system. The large broadening is thought to be due to Stark Broadening and shows that there is an extremely high ion and electron density in the plume[10].

The apparent breakdown of the liquid in this technique indicates that with certain solid liquid combinations some novel solids could be produced. It is hoped that this technique may allow crystalline carbon phosphide to be grown.

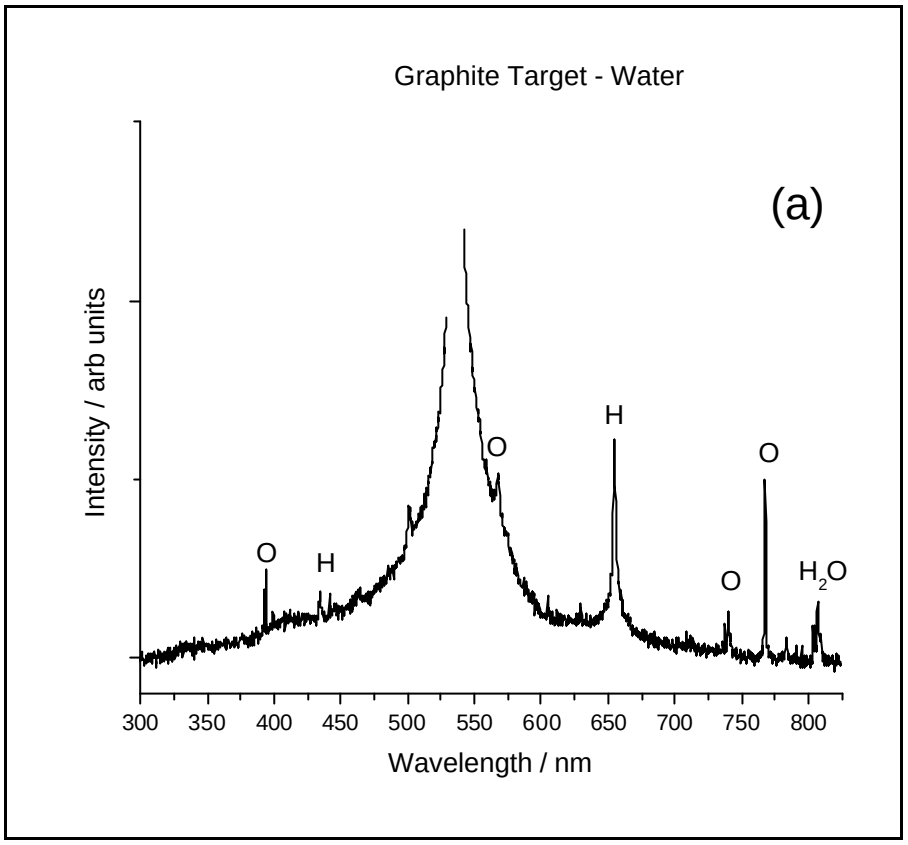

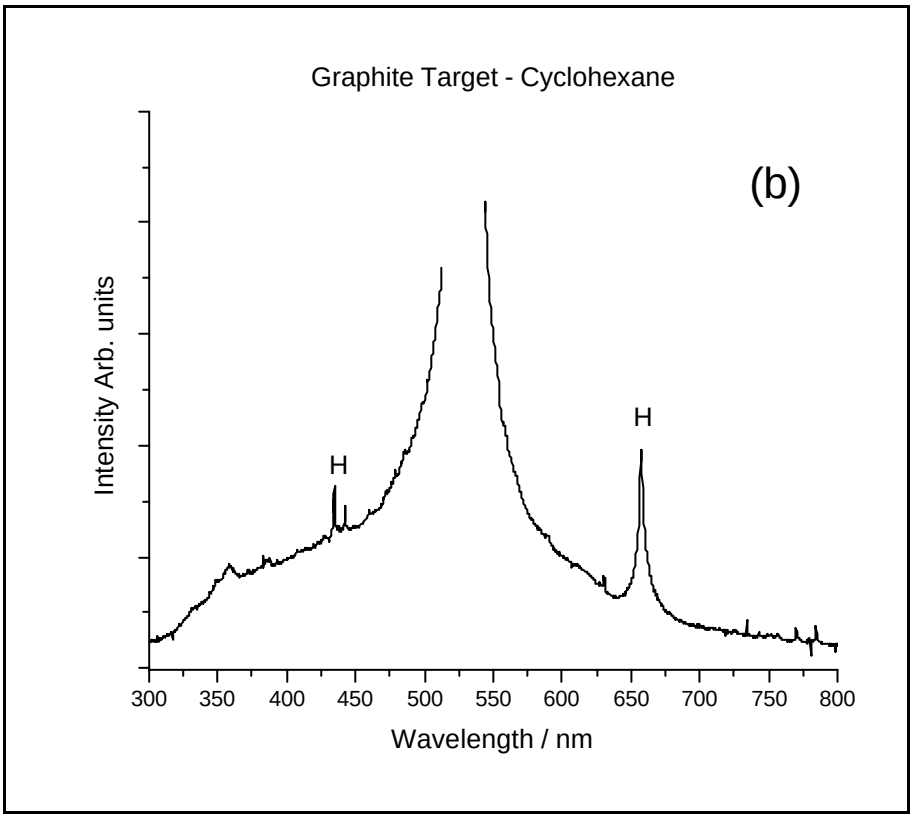

Figure 5.11: OES Spectra of the ablation plume from the ablation of (a) Graphite under water or (b) Graphite under cyclohexane

5.2 Phosphorus Ablated Under Carbon Containing Liquids

From the above results that show the liquid and solid are broken down into smaller particles and recombined into useful materials, it may be possible to use a different combination of solids and liquids to produce novel solids. In this case it may be possible to use a solid / liquid combination to produce carbon phosphide. As the predicted stable of structures of carbon phosphide are readily available, it is relatively simple to simulate the diffraction pattern from a number of these crystals. Elemental analysis of the suspensions was performed on the XPS, SIMS and EDX connected to the TEM. For samples that were being analysed by the TEM-EDX the support grid was made from SiO_2. For SAED work it was found more useful to use a carbon support grid. This will be discussed in more detail later.

5.2.1 The Ablation of Phosphorus Under Cyclohexane

In this study phosphorus was ablated under cyclohexane. Both red and white phosphorus were used. White phosphorus has a triclinic structure. This structure is shown in Figure 5.12. It has a low melting point (44.15 ^{o}C[11]). It is also extremely hazardous to use, ignites readily on contact with air and is highly toxic. As it has a crystalline structure it is difficult to distinguish other crystalline materials from it whilst working. The powder diffraction pattern for white phosphorus is shown in Figure 5.13.

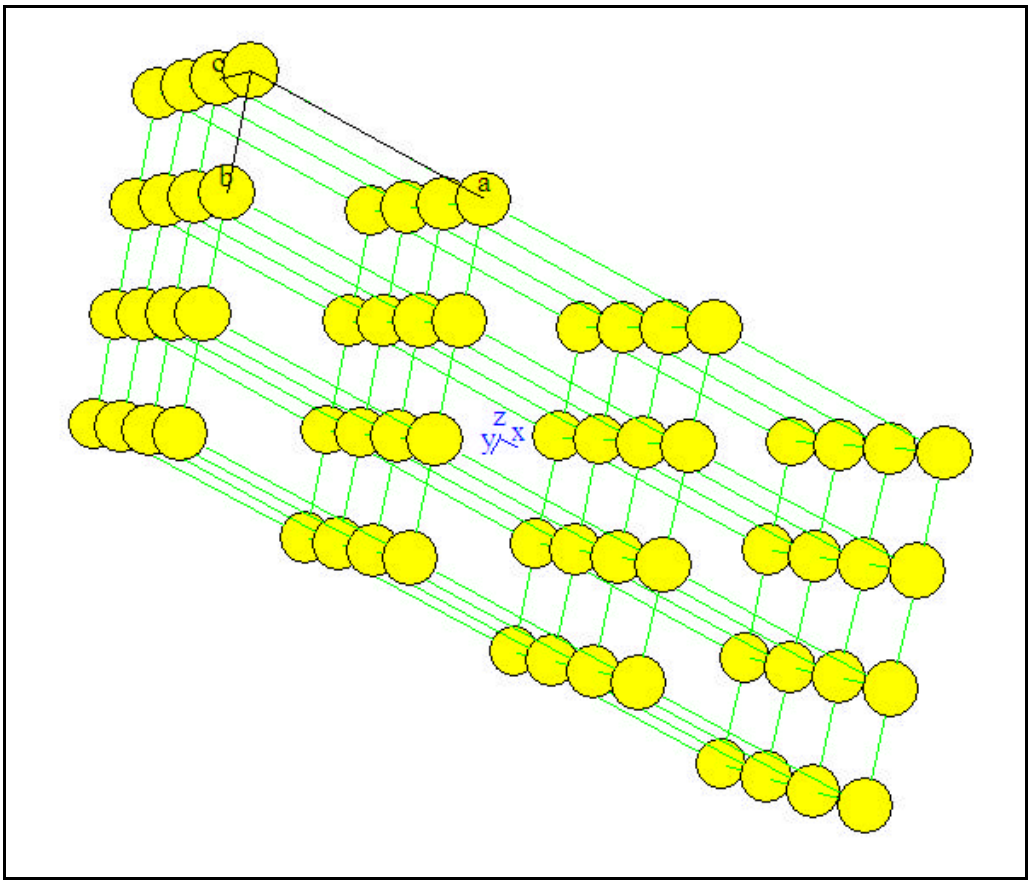

Figure 5.12: The triclinic structure of white phosphorus.

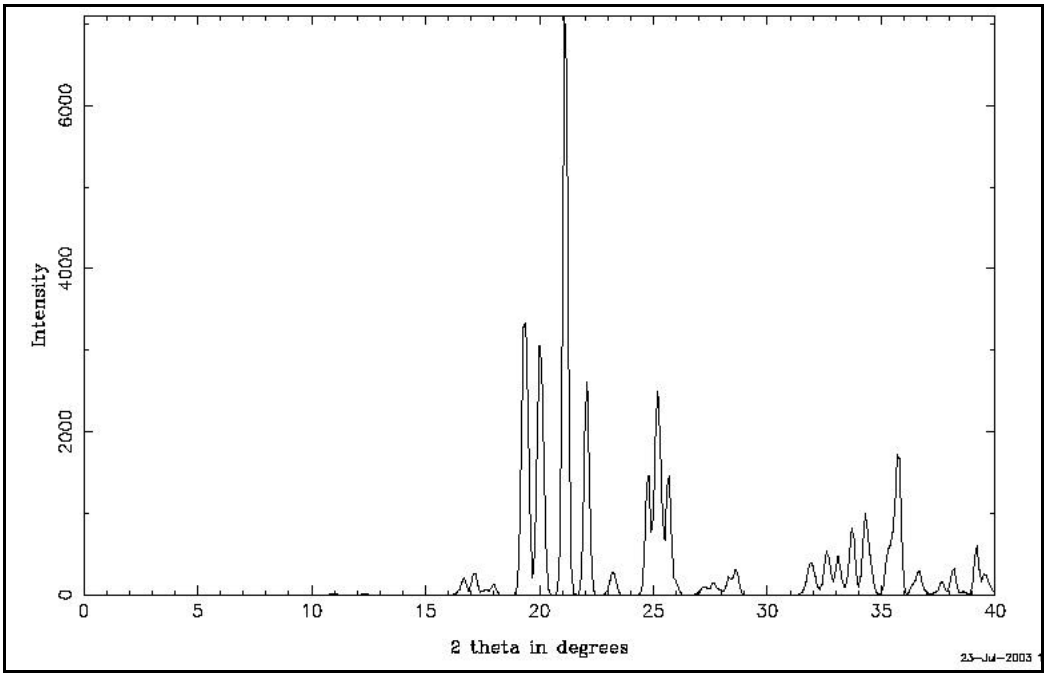

Figure 5.13: The powder diffraction pattern for white phosphorus from data obtained by Simon *et al*[12].

Red Phosphorus has a melting point of 590ºC[11], has an amorphous polymeric structure and is a lot safer to use than white phosphorus. It does not spontaneously combust in air and has a relatively low toxicity. As it is amorphous any crystalline material produced will be apparent from the TEM and SAED and can be identified easily. Cyclohexane has been chosen for the same reasons as in the previous section.

The simulations of the diffraction patterns of the structures proposed by Claeyssens, Lim and Zheng et al[13-16] are shown in Figure 5.14 (C_3P_4, pseudo cubic). The computer program CaRine has produced them. These are used as a comparison to any diffraction patterns obtained by the SAED of components in the products.

Suspensions made from red phosphorus ablated under cyclohexane had a transparent, yellow appearance. There were particles that could be seen, which if left overnight sunk to the bottom of the sample vial. Care was taken to ensure that the samples were agitated prior to analysis. When evaporating the liquid from the TEM grids in air a white smoke sometimes appeared above the sample or the pipette. It was thought that this was due to phosphorus oxides forming, as it is likely that some of the red phosphorus became white phosphorus in the ablation process (white and red phosphorus exist in an equilibrium at high temperatures). Care was therefore taken to ensure that samples were "pumped down" in the analysis chamber before the solvent was fully evaporated. Suspensions made from white phosphorus ablated under cyclohexane had a similar appearance, but had many more large particles in the suspension. This is thought to be because white phosphorus has a much lower melting and boiling point than red phosphorus it is ablated much more easily, with each laser pulse removing more material. Again like the red phosphorus samples the

TEM grid and pipette ‘smoked’ when the solvent dried. On several occasions the mixture caught fire. Again care had to be taken to ensure that not all of the solvent had been evaporated prior to pumping down for analysis. Samples made by the ablation of white phosphorus did not give any crystal diffraction patterns in the TEM so were not studied any further.

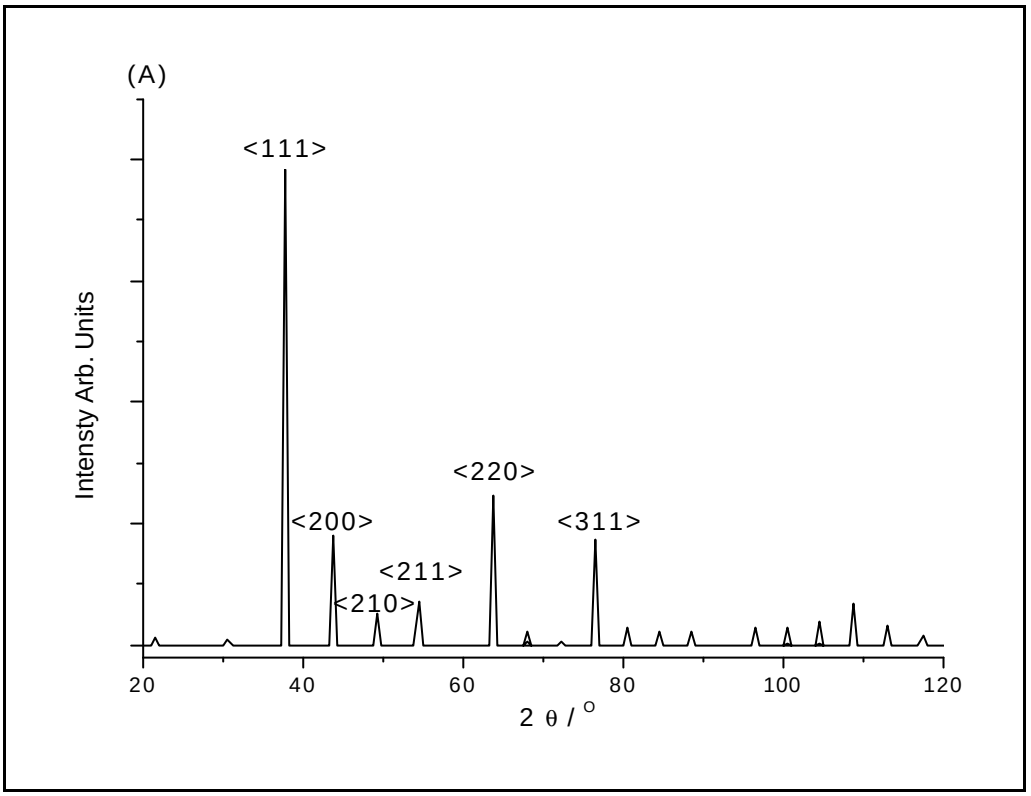

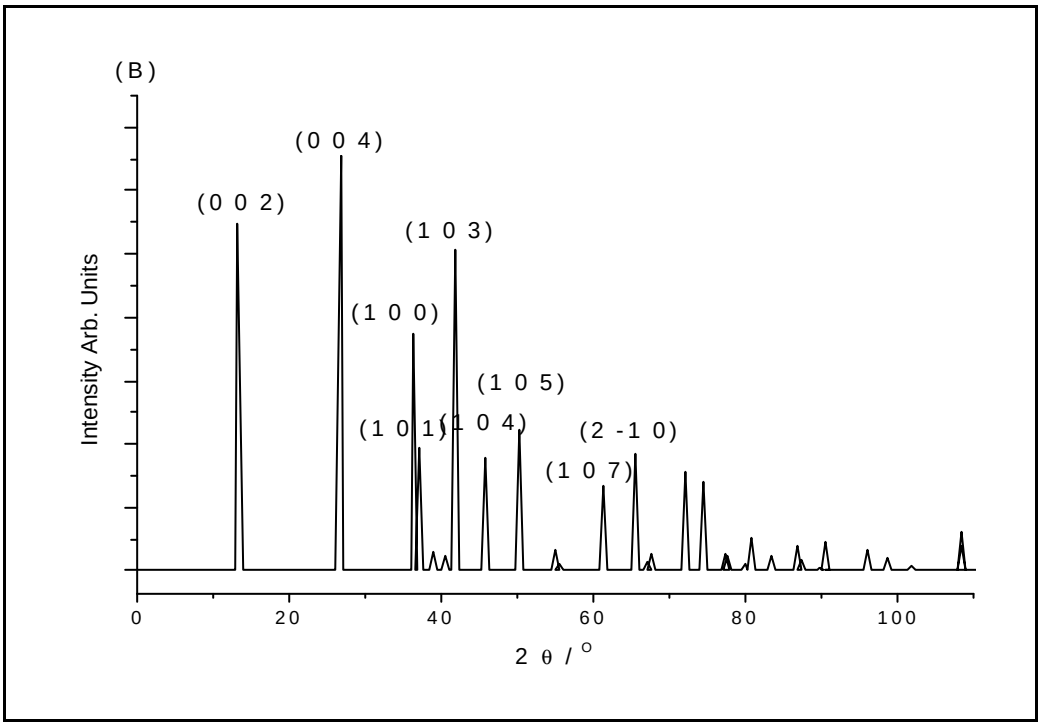

Figure 5.14: simulated diffraction patterns for the stable carbon phosphide structures proposed by Claeyssens, Lim and Zheng *et al*[13-16]. (A) Shows the diffraction pattern from the pseudo cubic structure (B) the GaSe like structure.

Electron microscopy (both scanning and transmission) revealed that the dried suspension contained many amorphous lumps. Figure 5.15 shows an SEM micrograph of the dried suspension, which was allowed to dry on a silicon wafer. The structure to the thin film is due to non-volatile components in the suspension. EDX showed that there was C, P and O present in the thin film. Figure 5.16 shows a feature found in a thin film. It is thought that this a piece of unreacted phosphorus. Indeed EDX spectroscopy of this area revealed a large amount of phosphorus concentrated in that area.

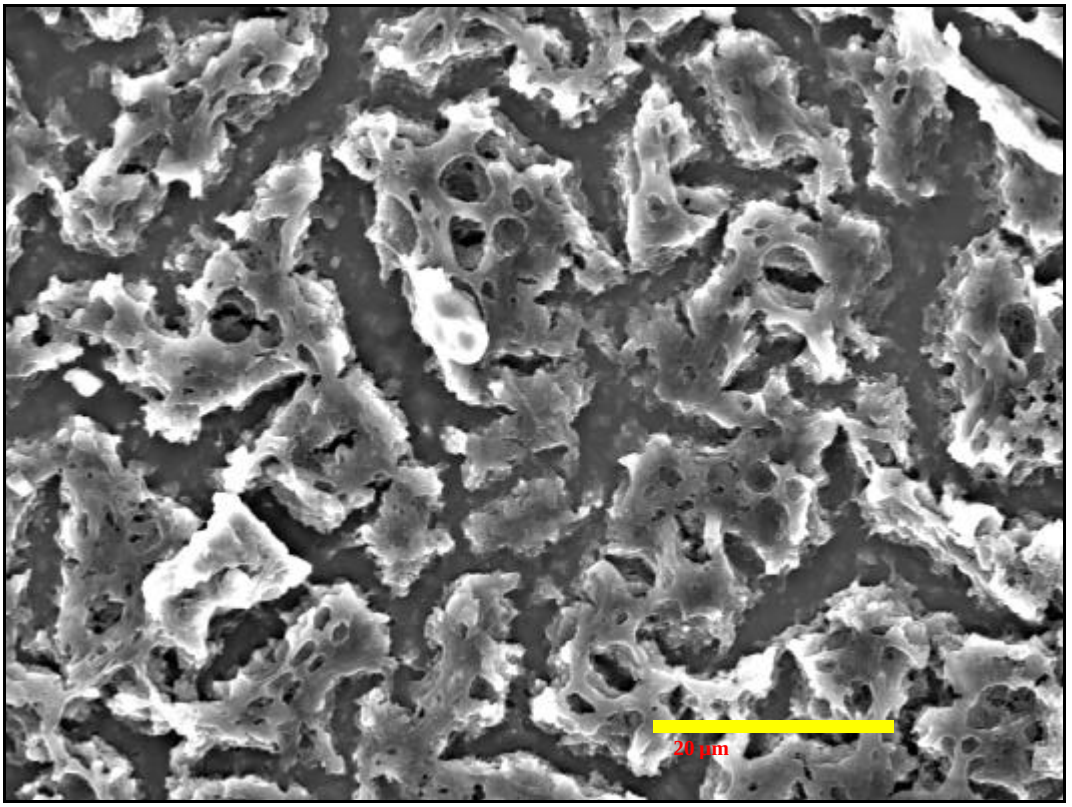

Figure 5.15: SEM micrograph of a dried suspension made by ablating red phosphorus under cyclohexane

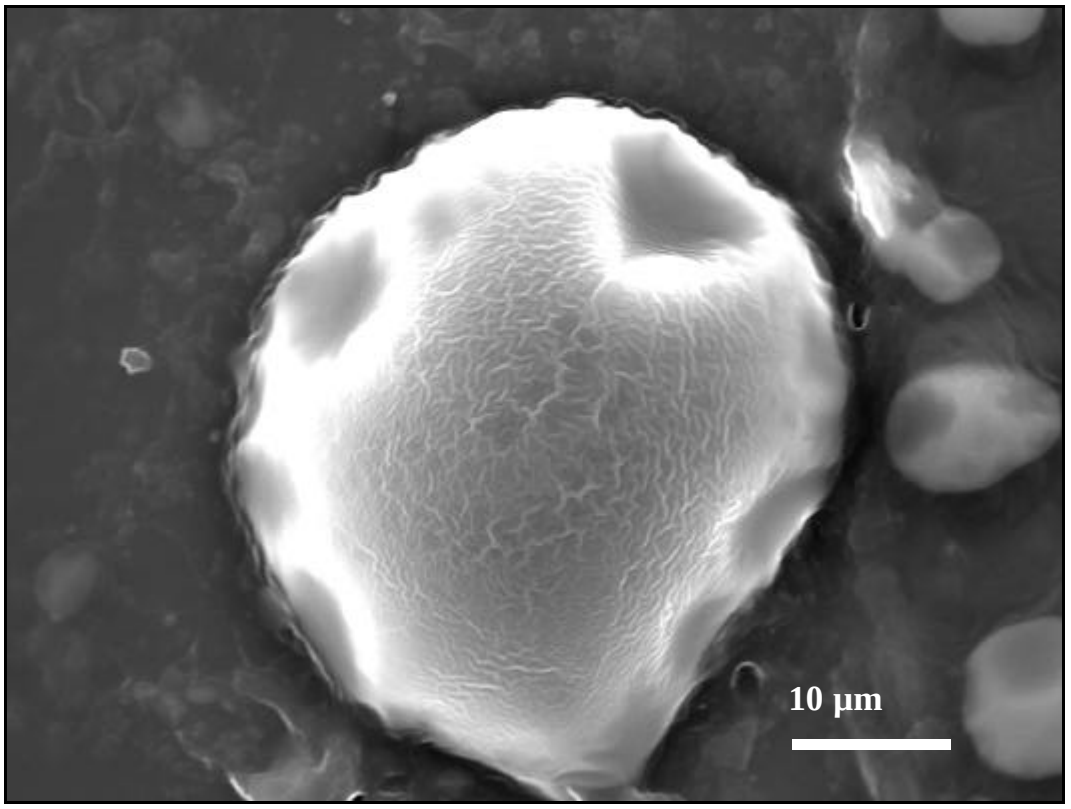

Figure 5.16: SEM micrograph of a feature found in the dried suspension produced by ablation of red phosphorus under cyclohexane.

XPS showed that the composition of the dried suspensions on Si wafer was 64.6% C, 9.4% P and 26% O. Figure 5.17 shows a SIMS spectrum of a dried suspension. It can instantly be seen that this spectrum is very different to spectra of thin films grown by RF-CVD. Firstly it is highly oxidised. Also the 43 amu peak is not as prominent. This is not suprising as the dried suspension will be a mixture of phosphorus, phosphorus oxides, breakdown products of cyclohexane and amorphous and (hopefully) crystalline forms of carbon phosphide. These results do not exclude carbon phosphide from having been made, but as the components of this mixture are very small (much lower than the spatial resolution of either the XPS or SIMS) it would not necessarily be seen.

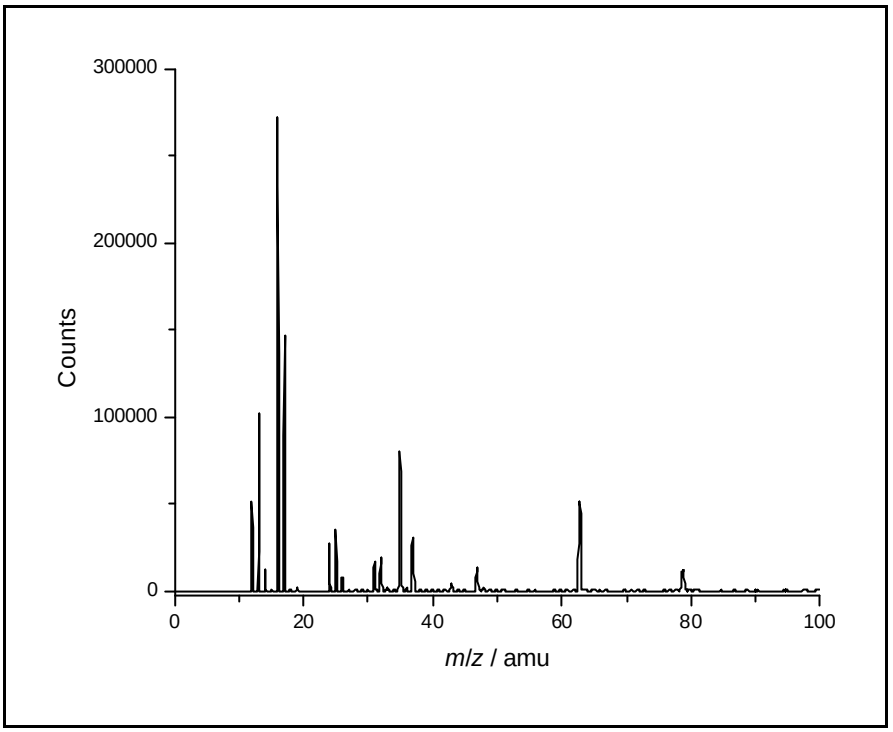

Figure 5.17: SIMS spectrum of a dried suspension produced by the ablation of red phosphorus under cyclohexane.

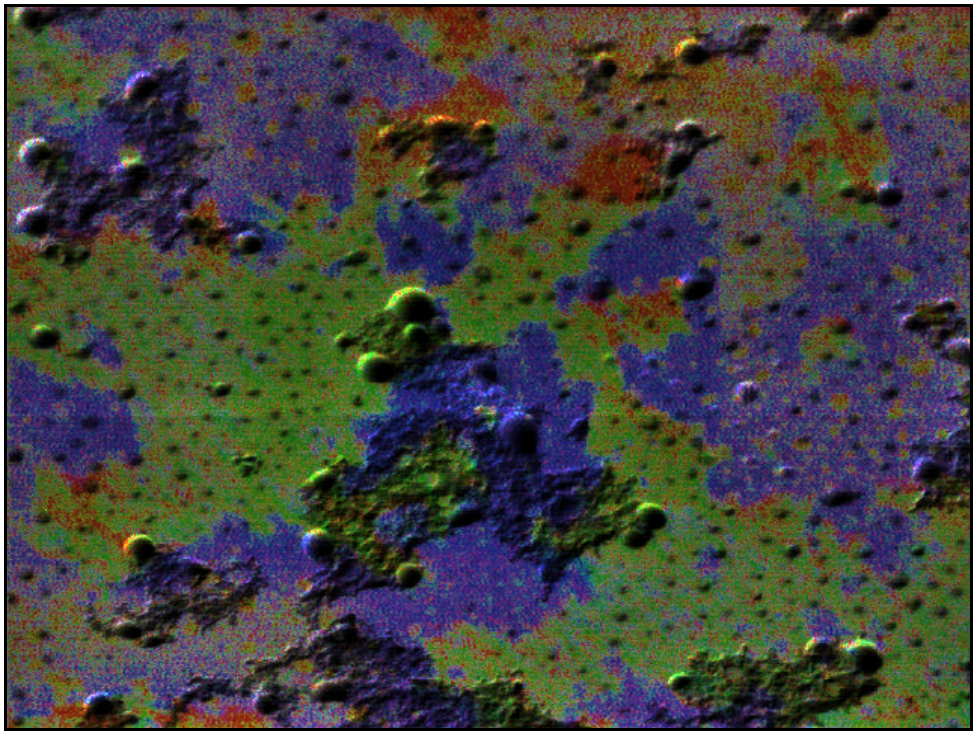

Figure 5.18: SIMS element map, backed by a secondary electron image of a dried suspension made by the ablation of red phosphorus under cyclohexane, the red represents *m/z* = 12 (C), the green represents *m/z*=42 (CP), the blue represents *m/z*=16 (O)

Figure 5.18 shows a SIMS element map of a dried red phosphorus/cyclohexane suspension. It can be seen that the CP areas and O areas are segregated. This shows that C and P are bonded together and that the C-P bonding is stable, preventing oxidation. This is similar to the results seen in the RF-CVD deposition of amorphous carbon phosphide. As the bonding between carbon and phosphorus increased the tendency for these films to oxidise decreased.

Figure 5.19 shows a TEM micrograph of some crystals found in a dried suspension made by the ablation of red phosphorus under cyclohexane. It can be seen that these crystals are very small (<100 nm). Figure 5.20 and Figure 5.21 show an SAED pattern and the radial intensity of the rings respectively. It can be seen that the radial intensity distribution of the SAED pattern is similar to the theoretical diffraction data shown in Figure 5.14 (the pseudo-cubic structure). To prove this the *d*-spacings and lattice parameter (*a* as $a=b=c$) can be checked against the diffraction data to ensure that they match against the theoretical data. As the system is pseudo-cubic the method for calculation is the same as above in Equation 5.3. For these data the four most prominent peaks will be checked against theoretical data, that is the peaks due to the <111>, <200>, <220> and <311> planes. Table 5.4 shows these results. The same peaks have been included for Cu, as Cu is a likely contaminant (the TEM grids and sample holder are made from Cu) and has a very similar crystal structure to the pseudo-cubic structure of carbon phosphide.

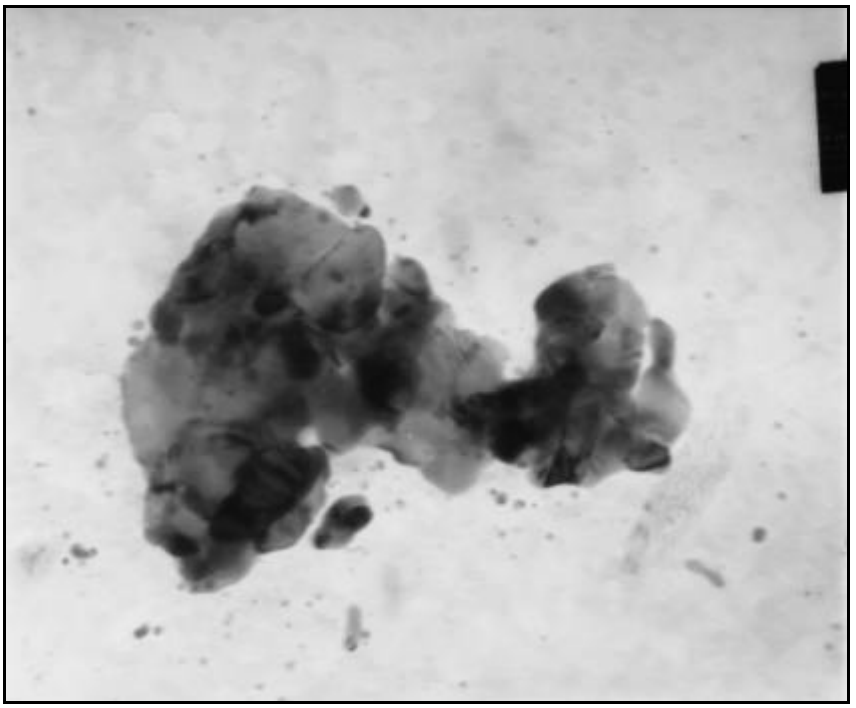

Figure 5.19: TEM micrograph of some crystals found in a suspension produced by ablation of red phosphorus under cyclohexane

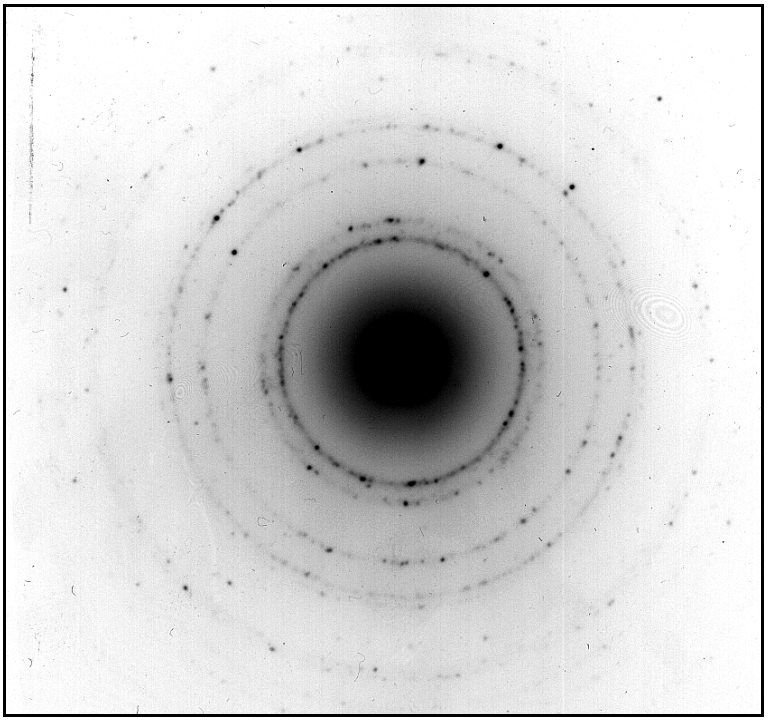

Figure 5.20: SAED of crystals found in a suspension produced by ablation of red phosphorus under cyclohexane

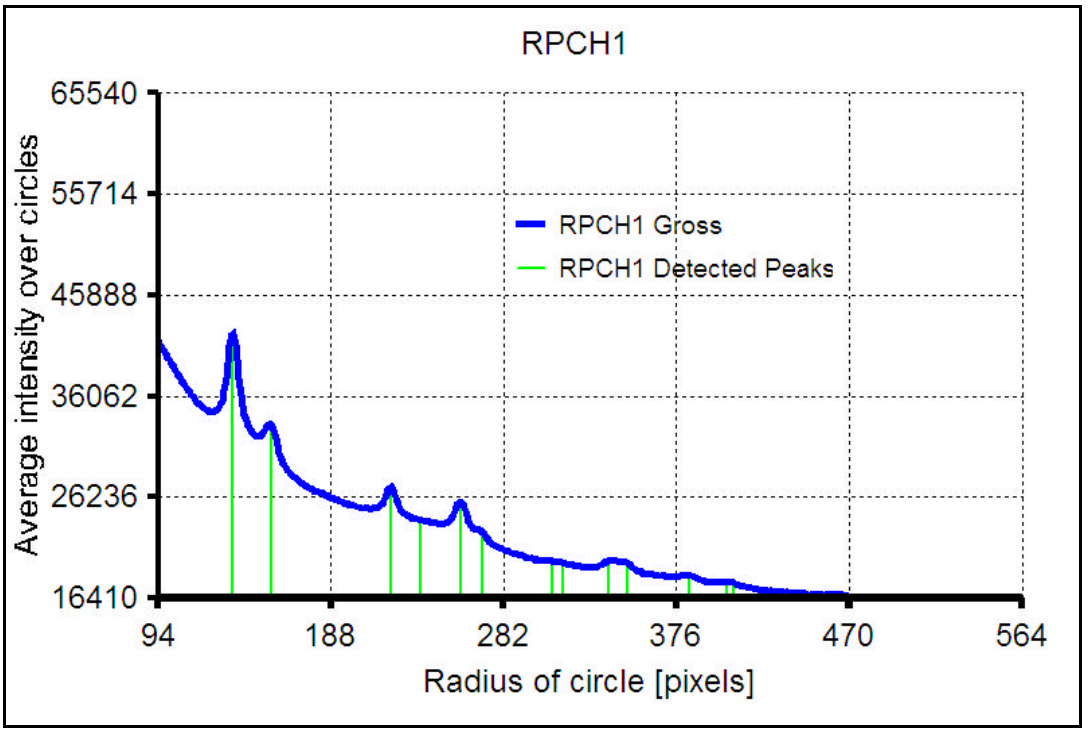

Figure 5.21: The darkness against the radius of the circle from the above SAED pattern, this was produced using Process Diffraction[4].

Plane	Experimental		Theoretical C_3P_4		Theoretical Cu	
	d-spacing	a / Å	d-spacing	a / Å	d-spacing	a / Å
<111>	2.31	4.01	2.384	4.13	2.09	3.61
<200>	2.00	4.00	2.065	4.13	1.81	3.62
<220>	1.41	3.99	1.46	4.13	1.28	3.61
<311>	1.20	3.99	1.245	4.13	1.09	3.62

Table 5.4: The plane spacings and lattice parameters for the crystals analysed by the SAED shown in Figure 5.20.

From Table 5.4 it can be seen that the SAED diffraction pattern matches closely with the theoretical data. Unfortunately at the time of obtaining this diffraction pattern EDX spectroscopy was not available on this TEM. Many subsequent attempts at repeating this experiment were not successful. Also on further attempts some Cu was found. A Cu film had its SAED taken, but the ring pattern gave *d*-spacings much closer to that of Cu on the same TEM. Unfortunately as this pattern has not been seen

when EDX facilities have been available it is not possible to prove whether or not it is crystalline carbon phosphide. But with the above evidence showing that there is CP bonding and how close a match the SAED data is, it is likely to be crystalline carbon phosphide. Reasons for why it has only been seen once will be discussed later in this section.

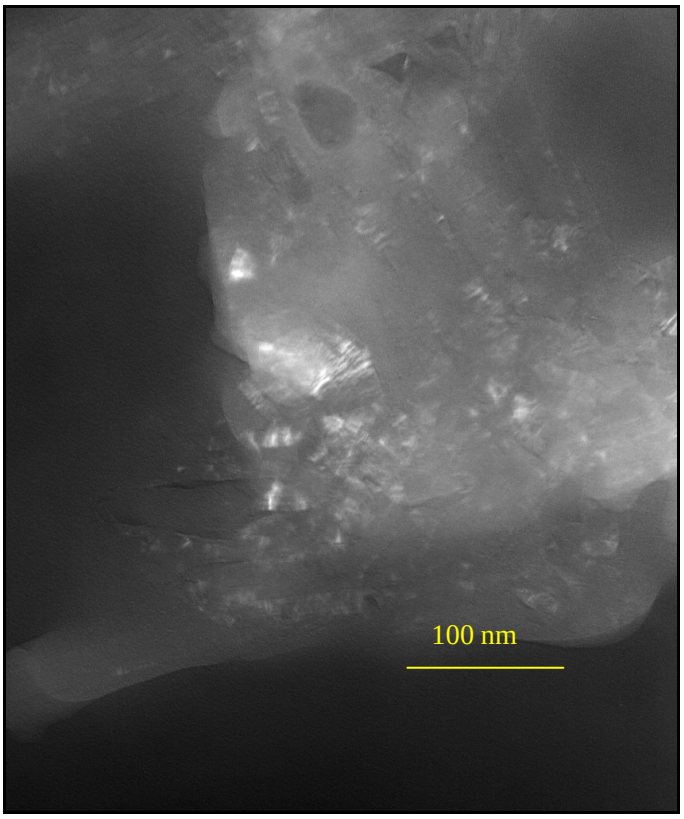

Figure 5.22: TEM Micrograph of some crystals found in a suspension made by ablation of red phosphorus under cyclohexane.

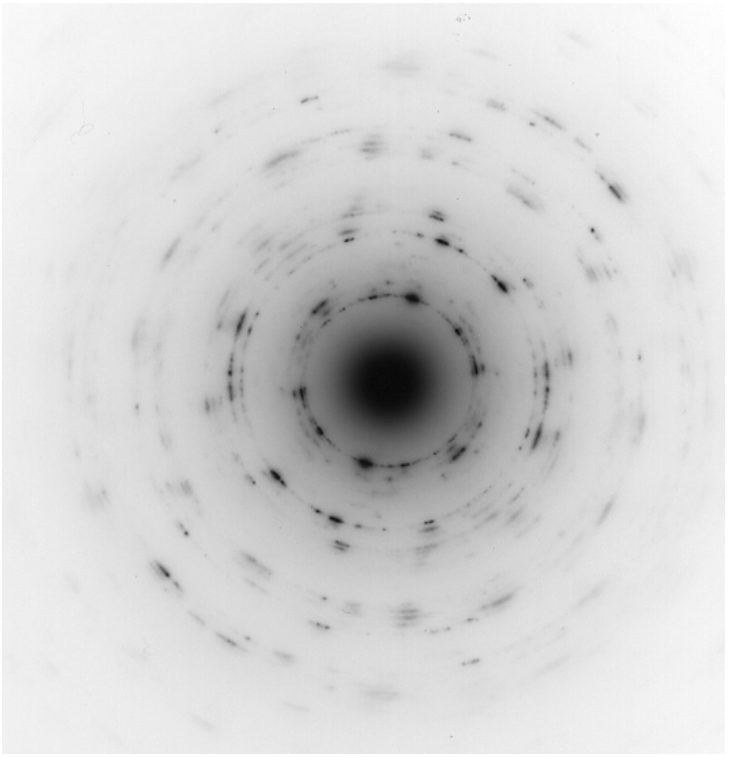

Figure 5.23: SAED pattern from the crystals shown in Figure 5.22.

Figure 5.22 and Figure 5.23 show some crystals found in a suspension produced by ablating red phosphorus under cyclohexane and an SAED ring pattern of those crystals. Analysis of the ring pattern by Process Diffraction was performed, but the inner three rings were too close together to be distinguished. So, the first *d*-spacing was found using Process Diffraction and the rest were worked out by using proportions of *r* for each ring, measured by hand:

$$d = \frac{ll}{r}$$

$$\therefore d \propto \frac{1}{r}$$

From the above equations it can be seen that *r* is inversely proportional to *d*. Therefore to work out the *n*th *d*-spacing (d_n):

$$d_n = \frac{d_1}{r_n / r_1}$$

Equation 5.4

Where d_1 is the first *d*-spacing, r_1 is the radius of the ring where the first *d*-spacing was calculated and r_n is the radius of the *n*th ring. For this SAED ring pattern the calculated *d*-spacings are listed in

Plane	*r* / mm	*d*-spacing / Å
<1 -1 0 0>	42	4.96
<0 0 0 2>	47	4.43
<1 -1 0 1>	49	4.25
<1 0 -1 2>	73	2.85
<1 1 -2 0>	78	2.67

Table 5.5. The ring pattern looks like a typical hexagonal close packed (HCP) system. For HCP systems $a = b \neq c$, this means that the calculation of the lattice parameters (*a* and *c*) is more difficult. A different indexing system is traditionally used in hexagonal crystal systems. These are Miller-Bravais indices.

The difference with this indexing system is that there are four sets of co-ordinates unlike the three sets used in the conventional Miller indexing system. This is for simplicity, in cubic and pseudo-cubic systems the unit cell is a cube, with all angles 90 º, this means that a 3-co-ordinate Cartesian like system is convenient. In hexagonal systems the unit cell is hexagonal, the cell can be indexed conveniently using a 4-co-ordinate system, *h, k, i and l*. Where *h*, *k* and *i* are in plane and point in the a_1, a_2 and a_3 directions (Figure 5.24), 120 º from each other. *l* is perpendicular to the plane and points towards *c*.

Plane	*r* / mm	*d*-spacing / Å
<1 -1 0 0>	42	4.96
<0 0 0 2>	47	4.43
<1 -1 0 1>	49	4.25
<1 0 -1 2>	73	2.85
<1 1 -2 0>	78	2.67

Table 5.5: The *d*-spacings of the crystals analysed by SAED in Figure 5.23

To work out the lattice parameters Equation 5.5 is used.

$$d = \sqrt{\frac{1}{(h^2 + k^2 + hk)\frac{4}{3a^2} + \frac{l^2}{c^2}}}$$

Equation 5.5

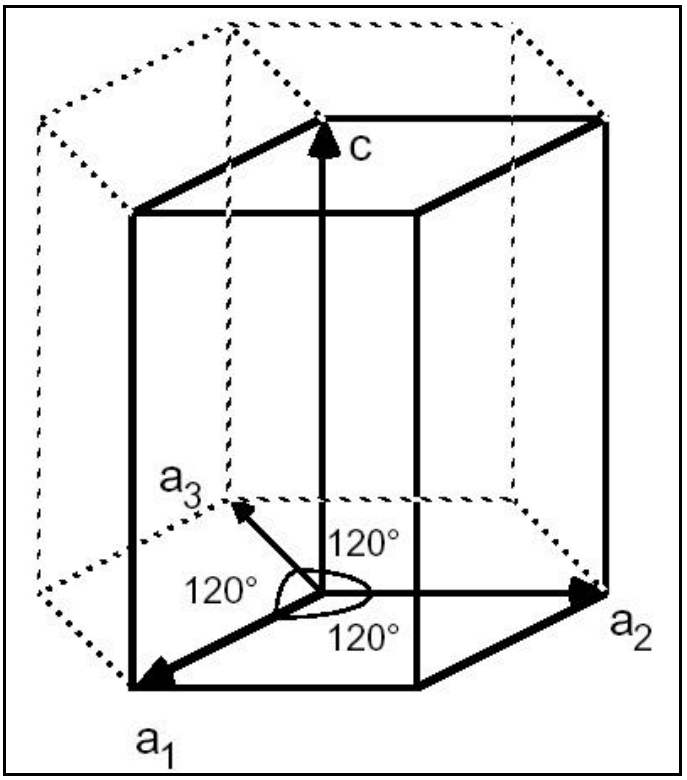

Figure 5.24: Picture illustrating the Miller-Bravais Indexing system for hexagonal crystals.

If the <1 –1 0 0> plane is being used Equation 5.5 becomes Equation 5.6:

$$d = \sqrt{\frac{1}{(1+1-1)\frac{4}{3a^2}+0}}$$

$$d = \sqrt{\frac{3a^2}{4}}$$

$$d = \frac{\sqrt{3}a}{2}$$

$$a = \frac{2d}{\sqrt{3}}$$

Equation 5.6

If the *d*-spacing for <1 –1 0 0> is substituted the lattice parameter *a* is found to be 5.73 Å. Substituting the data from the <0 0 0 2> ring will give *c*:

$$d = \sqrt{\frac{c^2}{2^2}}$$

$$d = \frac{c}{2}$$

$$c = 2d$$

Equation 5.7

Substituting the *d*-spacing for the <0 0 0 2> ring gives a *c* value of 8.86 Å. If the values of *a* and *c* are now substituted in and the *d*-spacings are calculated for these

data they can be compared to the experimentally calculated *d*-spacings and the HCP identification can be either confirmed or rejected. Table 5.6 shows this:

Plane	Calc *d*-spacing / Å	Exp *d*-spacing / Å
<1 –1 0 0>	4.96	4.96
<0 0 0 2>	4.43	4.43
<1 –1 0 1>	4.33	4.25
<1 0 -1 2>	3.31	2.85
<1 1 -2 0>	2.86	2.67

Table 5.6: Experimentally determined *d*-spacings and calculated *d*-spacings for this crystal

The fit of this data is similar to the theoretical data, especially if the experimental <1 0 –1 2> data are substituted for the <1 1 –2 0>. This is valid as the <1 0 –1 2> may just not be visible on this pattern. The values of *a* and *c* do not match up with the GaSe structure proposed by Zheng *et al*[15]. This does not necessarily exclude the structure though, as the value of *a* is nearly exactly double the number calculated by Zheng *et al* (Zheng *et al* calculated *a* as 2.85 Å and *c* as 13.389 Å). There may be two units of slightly different arrangement in one unit cell. Also for hexagonal crystals the theoretical calculation of *c* is not reliable. Unfortunately these results have only been observed once and the TEM did not have a working EDX, so it cannot be proven either way.

It is important to discuss why these crystals have only been seen on a small number of occasions. In the transformation of graphite into diamond case above, most of the solid remained untransformed and remained as graphite. It was difficult to find diamond. In this case the graphite was the only component to undergo the transformation so even though diamond was scarce it could be found with relative ease. In the case of the synthesis of carbon phosphide both the liquid and solid have

to be broken down and react with each other. As <5% of the graphite became diamond the likelihood of the phosphorus and solvent reacting together is much lower. If this is coupled with the fact that magnifications of >100 000 were needed to see the crystals that were found the likelihood of finding crystals is very low. A typical TEM grid has a diameter of 3 mm. At 100 000 magnification 3 mm is equivalent to 300 m. A typical crystal is 100 nm. 100 nm at 100 000 magnification is equivalent to 1 mm. Searching for crystals is a lot like searching for several very small needles in an enormous haystack.

It was found that crystals were only ever observed in samples that were deposited at the maximum laser power and with a very tight focus. This shows that high fluence was very important in the production of these crystals. Unfortunately the laser being used in this study was rather old and not as powerful as it might be. Perhaps an increase in laser power may have the effect of producing more crystals. The laser wavelength was changed to the Nd:Yag fundamental at 1064 nm. As the laser did not have to pass through a frequency doubling crystal much higher fluences were obtained. Samples deposited at this wavelength did not turn yellow and the suspension sank totally to the bottom of the vial very quickly. The suspension was composed of phosphorus pieces that were chipped from the phosphorus target and there was no crystalline material found, even if the fluence was set to the same fluence as the 532 nm deposition. This shows that high fluence at shorter wavelengths may have the desired effect. Unfortunately the equipment to test this theory was not available.

5.2.2 Ablation of Phosphorus Under Xylene

The ablation of red phosphorus under xylene was performed due to there being less H in the xylene molecule, but xylene is not as hazardous as benzene or toluene. On ablation under xylene the suspension was transparent, but a very dark brown colour. It was thought that this was because of the double bonds in the aromatic ring breaking and forming coloured compounds. TEM of the suspensions revealed no crystalline material.

Figure 5.25 shows a SIMS spectrum of a sample of the dried suspension. There are a number of peaks due to C containing species, P containing species and O containing species. Again like in the cyclohexane case there is a very small peak at 43 amu due to CP. Figure 5.26 shows a SIMS element map that shows, like the cyclohexane case, the CP and oxidised species are staying separate.

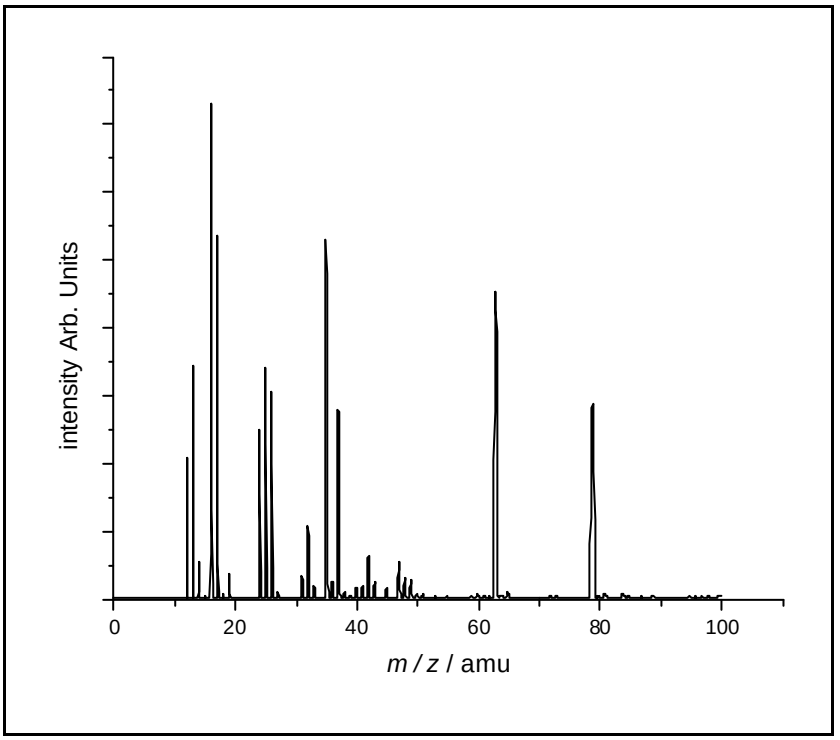

Figure 5.25: SIMS spectrum of a dried suspension produced by the ablation of red phosphorus under xylene.

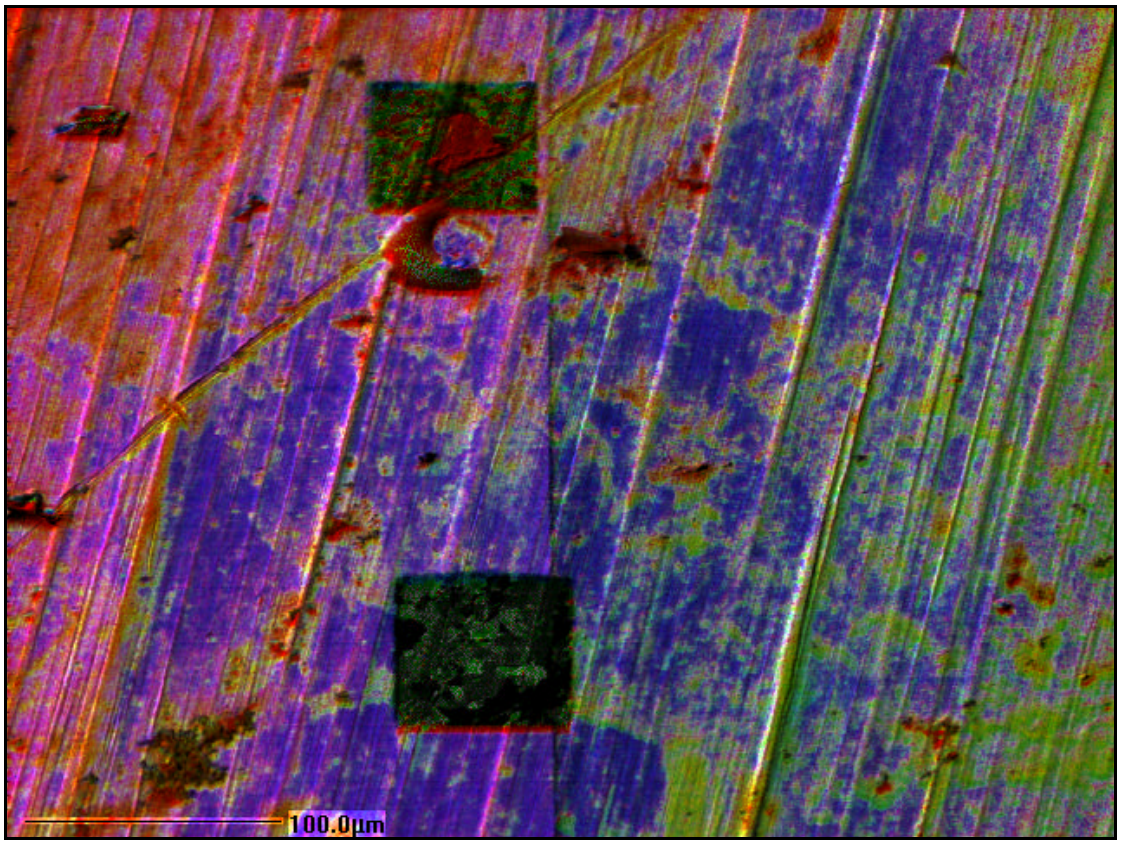

Figure 5.26: SIMS element map of a sample of dried suspension made by ablation of red phosphorus under xylene. The red represents *m/z* = 12 (C), the green represents *m/z*=42 (CP), the blue represents *m/z*=16 (O).

Unfortunately as there were no crystals found there was no further analysis of samples made in this way. But analysis of the existing samples does show the C and P are present and are bonding together. This is in an amorphous manner such as found in the thin films deposited in the previous chapter.

5.2.3. Ablation of mixed (red phosphorus/graphite) targets under cyclohexane.

In this study the solid target was a 1:1 mixture of red phosphorus powder and graphite powder pressed into a pellet as described in the experimental section. The reason for this was that the process would not have to rely on the reaction of the liquid, only the target onto which the laser was focused was needed to react. It was hoped that the

target was homogenous enough to allow ablation of both carbon and phosphorus in the same shot, hence allowing carbon and phosphorus to react in the high-pressure ablation plume.

After ablation the samples had the yellow transparent appearance that was always seen with cyclohexane samples. The samples also had a lot of suspended solid. It was thought that this was mostly the graphite and red phosphorus from the targets (the laser ablation process broke them up well). This was confirmed with TEM. TEM analysis of these samples was difficult as there was a lot of crystalline material present on the TEM grid, again most of this was graphite. There was also amorphous material. It was thought that this was either amorphous carbon phosphide or red phosphorus.

Figure 5.27 shows an SAED pattern from some crystals found in the suspension. It can be seen that it looks very similar to the diamond ring patterns seen in section 5.1. Indeed the *d*-spacings and lattice parameter correspond well to diamond. It is likely that due to the environment which this has been grown in that this diamond has a high P concentration. Unfortunately due to a high background concentration it was not possible to prove this using EDX spectroscopy.

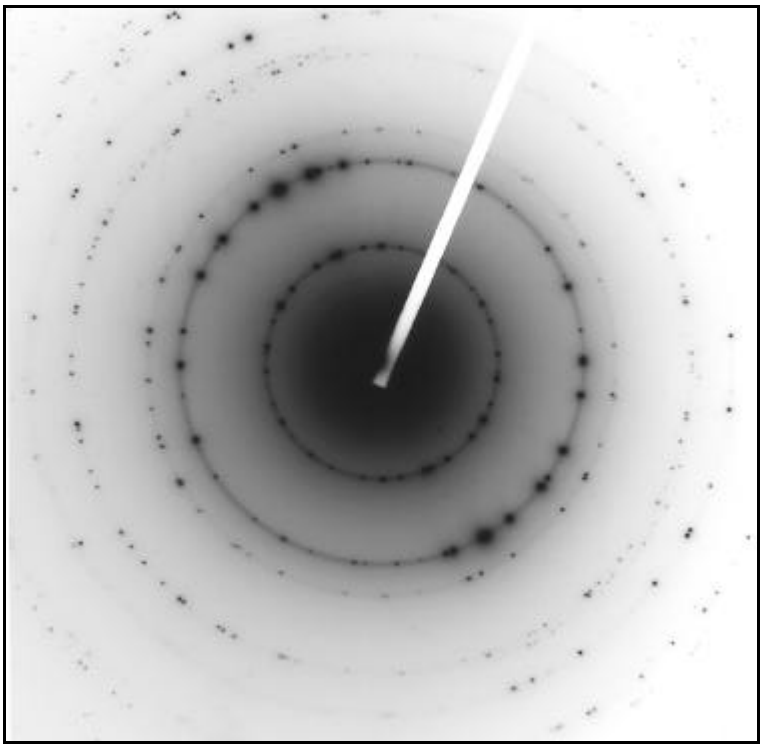

Figure 5.27: SAED pattern of some crystals found in a dried suspension made by the ablation of mixed targets under cyclohexane.

The ablation of phosphorus under various solvents may have been successful in making crystalline carbon phosphide. This is only on very small amounts and it is not proven. No electrical or other properties can be measured from such a dilute amount. But this study does pave the way for future studies. With a refinement of the experimental technique and a more powerful laser I am confident that crystalline carbon phosphide will be made by this method.

References

1 G. W. Yang and J. B. Wang, Applied Physics a-Materials Science & Processing **72,** 475-479 (2001).

2 G. W. Yang, J. B. Wang and Q. X. Liu, Journal of Physics: Condensed Matter **10,** 7923-7927 (1998).

3 J. B. Wang, C. Y. Zhang, X. L. Zhong and G. W. Yang, Chemical Physics Letters **361,** 86-90 (2002).

4 J. L. Lábár, in *Proceedings of EUREM 12*; *Vol. 3*, edited by L. Frank and F. Ciampor (2000), p. I379-380.

5 C. Boudias and D. Monceau, 3.1 ed. (Divergent S.A., Compiegne, France, 1998).

6 J. Fayos, Journal of Solid State Chemistry **148,** 278-285 (1999).

7 K. Toyota, T. Tanaka, S. Nishiwaki, S. Nakashima and T. Okada, Journal of Photochemistry and Photobiology a-Chemistry **141,** 9-16 (2001).

8 S. Prawer, K. W. Nugent, D. N. Jamieson, J. O. Orwa, L. A. Bursill and J. L. Peng, Chemical Physics Letters **332,** 93-97 (2000).

9 R. Pfeiffer, H. Kuzmany, P. Knoll, S. Bokova, N. Salk and B. Gunther, Diamond and Related Materials **12,** 268-271 (2003).

10 H. R. Griem, Contributions to Plasma Physics **40,** 46-56 (2000).

11 *CRC Handbook of Chemistry and Physics*, 14 ed. (CRC Press, New York, USA, 1992).

12 A. Simon, H. Borrmann and H. Craubner, Phosphorus and Sulfur **30,** 507-510 (1987).

13 F. Claeyssens, J. M. Oliva, P. W. May and N. L. Allan, International Journal of Quantum Chemistry **In Press** (2003).

14 F. Claeyssens, N. L. Allan, P. W. May, P. Ordejon and J. M. Oliva, Chemical Communications**,** 2494-2495 (2002).

15 J. C. Zheng, M. C. Payne, Y. P. Feng and A. T. L. Lim, Physical Review B **67,** art. no.-153105 (2003).

16 A. T. L. Lim, J. C. Zheng and Y. P. Feng, International Journal of Modern Physics B **16,** 1101-1104 (2002).